Selective Inhibitors of the JMJD2 Histone Demethylases: Combined Nondenaturing Mass Spectrometric Screening and Crystallographic Approaches[†]

Nathan R. Rose,[‡] Esther C. Y. Woon,[‡] Guy L. Kingham,[‡] Oliver N. F. King,[‡] Jasmin Mecinović,[‡] Ian J. Clifton,[‡] Stanley S. Ng,[§] Jobina Talib-Hardy,[‡] Udo Oppermann,[§] Michael A. McDonough,[‡] and Christopher J. Schofield*,[‡]

[‡]*The Department of Chemistry and the Oxford Centre for Integrative Systems Biology, Chemistry Research Laboratory, University of Oxford, 12 Mansfield Road, Oxford, OX1 3TA, United Kingdom, and* [§]*Structural Genomics Consortium, University of Oxford, Old Road Campus Roosevelt Drive, Headington OX3 7DQ, United Kingdom, The Botnar Research Centre, Oxford Biomedical Research Unit, Oxford OX3 7LD, United Kingdom*

Ferrous ion and 2-oxoglutarate (2OG) oxygenases catalyze the demethylation of N^ε-methylated lysine residues in histones. Here we report studies on the inhibition of the JMJD2 subfamily of histone demethylases, employing binding analyses by nondenaturing mass spectrometry (MS), dynamic combinatorial chemistry coupled to MS, turnover assays, and crystallography. The results of initial binding and inhibition assays directed the production and analysis of a set of *N*-oxalyl-D-tyrosine derivatives to explore the extent of a subpocket at the JMJD2 active site. Some of the inhibitors were shown to be selective for JMJD2 over the hypoxia-inducible factor prolyl hydroxylase PHD2. A crystal structure of JMJD2A in complex with one of the potent inhibitors was obtained; modeling other inhibitors based on this structure predicts interactions that enable improved inhibition for some compounds.

Introduction

Histone lysine methylation is a dynamic post-translational modification, with sequence-specific *N*-methyltransferases and demethylases acting to add and remove methyl groups (Figure 1).[1] The methylation (or demethylation) of specific lysine residues can enable both euchromatic or heterochromatic states, thus transcriptionally activating or silencing genes. Histone demethylases (HDMs[a]) are implicated in diseases including leukemia, prostate cancer, squamous cell carcinoma, and X-linked mental retardation.[2] The largest identified family of HDMs is the JmjC-domain-containing family, the members of which are Fe(II) and 2-oxoglutarate (2OG) dependent oxygenases.[3,4]

The human JMJD2 HDM subfamily has six members (JMJD2A, 2B, 2C, 2D, 2E, and 2F), of which JMJD2A-C have been shown to catalyze demethylation of the methylated forms of histone 3 lysine 9 (H3K9) and histone 3 lysine 36 (H3K36) in vitro and in cells, while JMJD2D is selective for the demethylation of H3K9.[4−7] JMJD2C has been implicated in prostate cancer, and inhibition of JMJD2C expression has been shown to decrease cancer cell proliferation.[4] Although

JMJD2E has been classified as a pseudogene,[8] recombinant JMJD2E has HDM activity, and is amenable to inhibition studies.[9] JMJD2F has not been characterized.

The precise in vivo roles of individual HDMs in the regulation of gene expression are unclear or only beginning to emerge. A degree of redundancy likely exists, with different demethylases targeting the same histone methyllysines. Small molecule chemical probes may be useful for investigating the in vivo role of these demethylases,[10] and the therapeutic potential of HDM inhibitors is being considered.[11] To be useful as probes, HDM inhibitors should not inhibit at least some of the other Fe(II)/2OG dependent oxygenases, e.g., those involved in the hypoxic response pathway, including the hypoxia-inducible factor (HIF) asparaginyl hydroxylase, factor-inhibiting HIF (FIH), and the human HIF prolyl hydroxylase domain 2 (PHD2), because the activity of these enzymes regulates a large array of human genes.[12−14]

Recently, we reported screening methods and several HDM inhibitor "scaffolds" for the JMJD2 HDM subfamily.[9] Compounds analyzed included the known histone deacetylase inhibitors suberoylanilide hydroxamic acid (SAHA), trichostatin A (TSA), pyridine-dicarboxylic acids, and various other 2OG analogues. The latter included *N*-oxalyl-D-phenylalanine **1d**, which has previously been shown to be selective for the inhibition of FIH with respect to PHD2;[15] this selectivity was achieved by exploiting a hydrophobic subpocket adjacent to the 2OG binding site present in FIH but not in PHD2. FIH has been regarded as part of the Jmj subfamily of 2OG dependent oxygenases[6,16,17] and is more similar in sequence and structure to the JMJD demethylases than it is to other human 2OG oxygenase subfamilies.[12]

Crystallographic studies and modeling imply that the JMJD2s possess a similar subpocket to that observed for FIH,
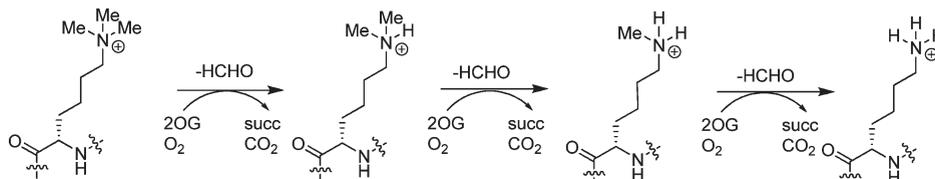

Figure 1. Reactions catalyzed by the JMJD2 histone demethylases. Each step is coupled to the conversion of O_2 and 2-oxoglutarate to succinate and CO_2. 2OG = 2-oxoglutarate, succ = succinate.

which is adjacent to the active site.[15,18] However, the crystallographic analyses imply that the subpocket of the JMJD2s is significantly larger and more open than that of FIH and extends into the substrate binding groove. We set out to explore this subpocket by derivatization of *N*-oxalyl-D-phenylalanine **1d** as a possible means of achieving selectivity toward the JMJD2 subfamily. We used a combined approach employing binding assays using nondenaturing mass spectrometry, disulfide exchange based dynamic combinatorial chemistry, inhibition studies, and crystallographic analyses, which led to the identification of *N*-oxalyl-D-tyrosine derivatives as potent inhibitors of JMJD2E.

Results

Initially, we used nondenaturing electrospray ionization mass spectrometry (ESI-MS) to assess binding of potential inhibitors to JMJD2E.[19] When the target protein is amenable to such assays, the stoichiometry of interaction and binding strength can be rapidly assessed. This method has been used in the study of metallo-enzyme inhibition (e.g., refs 20, 21) and enzyme−metal ion interactions.[22] In these ESI-MS analyses, it is important to appreciate that different types of noncovalent interaction survive the transition from solution to gas-phase differently (for review, see ref 6). However, in some cases, including metallo-enzymes,[20−25] good agreement between results from nondenaturing ESI-MS binding data and solution-phase data can occur.

Our starting points for the binding assay were the 2OG analogues that we had identified in the initial study aimed at identifying "template" inhibitors of JMJD2E suitable for derivatization, in particular *N*-oxalylglycine **1a** ($IC_{50} = 24\ \mu M$) and *N*-oxalyl-D-homophenylalanine **1h** ($IC_{50} = 39\ \mu M$).[9] A set of *N*-oxalyl-D-amino acids **1b−g** and their corresponding L-isomers **1i−n** were assessed for potential binding to the JMJD2E·Fe(II)·Zn(II) complex (hereafter JMJD2E) (Figure 2) by nondenaturing ESI-MS screening. The results revealed that of the 13 compounds tested, *N*-oxalylglycine **1a** and *N*-oxalyl-D-cysteine **1b** bound to JMJD2E (41256 Da), with formation of new peaks at 41403 and 41448 Da, corresponding to JMJD2E·**1a** and JMJD2E·**1b** complexes, respectively. Relatively weak binding was observed for *N*-oxalyl-D-phenylalanine **1d** (JMJD2E·**1d**: 41493 Da), *N*-oxalyl-D-valine **1f** (JMJD2E·**1f**: 41445 Da), and *N*-oxalyl-D-alanine **1g** (JMJD2E·**1g**: 41417 Da). These observations were in general agreement with the formaldehyde dehydrogenase (FDH) coupled assay inhibition results (measuring JMJD2E turnover with a histone H3 Lys9 trimethylated (H3K9me3) peptide fragment substrate) (Table S1, Supporting Information). It is notable that while some of the *N*-oxalyl-D-amino acids are active, none of the L-compounds **1i−n** bind to JMJD2E, and all, with the exception of **1n** ($IC_{50} = 285\ \mu M$), are inactive as inhibitors in FDH coupled assays. The importance of the D-stereochemistry in the *N*-oxalyl amino acid series is demonstrated by the significantly greater potency of *N*-oxalyl-D-cysteine **1b** ($IC_{50} = 73\ \mu M$) compared
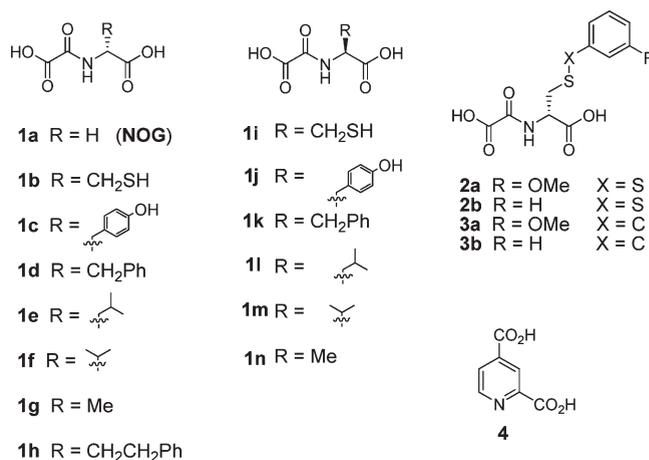

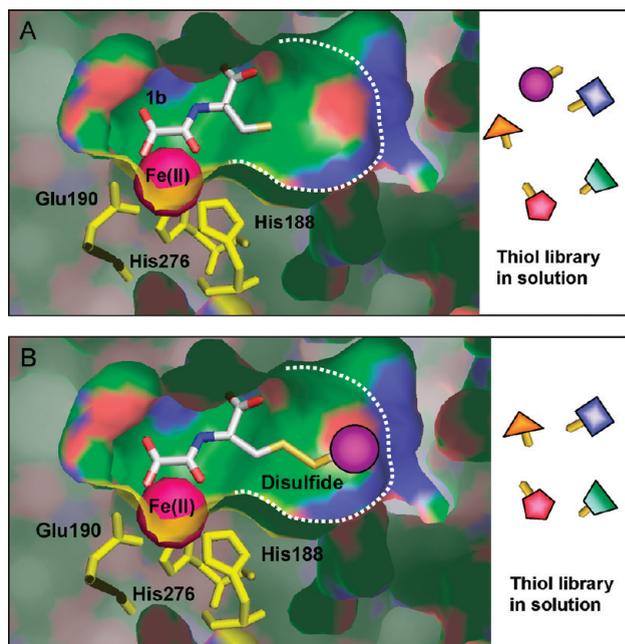**Figure 2.** Structures of potential inhibitors used in this study.

Figure 3. Dynamic combinatorial mass spectrometry (DCMS) approach. (A) The *N*-oxalyl group of support ligand **1b** anchors the molecule into the active site of JMJD2E via interaction with the Fe(II) ion (magenta), leaving the thiol side chain free for disulfide formation with the thiol library in solution. (B) Selective formation of a JMJD2E−disulfide complex with the thiol member that fits best into the active site.

to *N*-oxalyl-L-cysteine **1i** ($IC_{50} > 1$ mM) for inhibition of JMJD2E.

To explore the extent of the JMJD2E 2OG-substrate binding pocket that is accessible to the *N*-oxalyl amino acid series, a disulfide exchange based dynamic combinatorial-mass spectrometry (DCMS) screen[21,24,26] was then performed. The
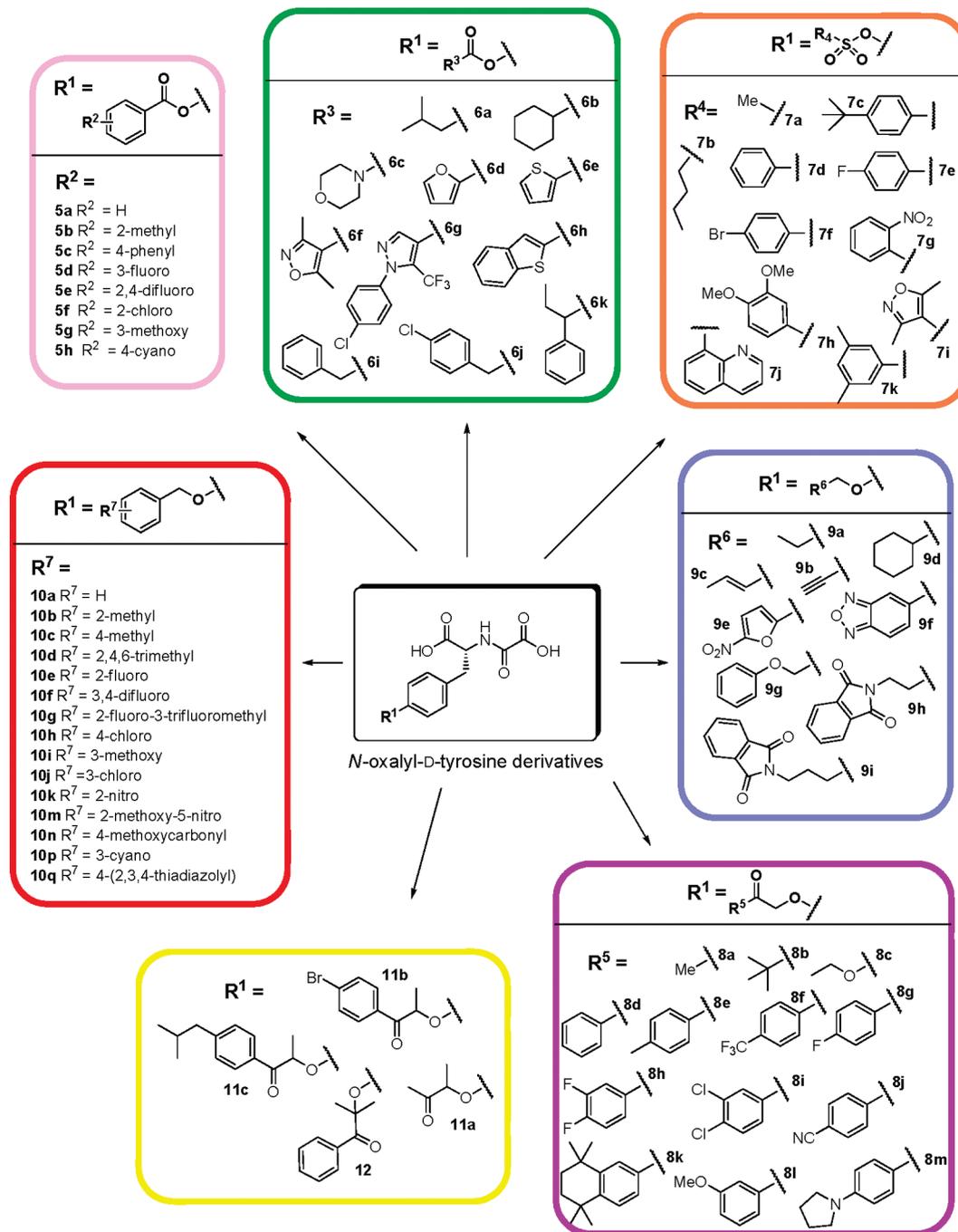
Figure 4. Structures of the *N*-oxalylamino acids investigated in this study.

DCMS screen exploited the thiol side chain of *N*-oxalyl-D-cysteine **1b,** which is predicted to project into the subpocket of JMJD2E as a "support" ligand (Figure 3). In this method, a compound that binds to the active site (the support ligand) which contains a thiol is allowed to react (either on the enzyme in the active site, or in solution) with a set of thiols to form a mixture of disulfides. Nondenaturing ESI-MS is then used to analyze which disulfides bind preferentially to the enzyme.

A mixture of five thiols, each thiol at 15 μM, including thiophenol, 3-bromothiophenol, 3-methoxythiophenol, propanethiol, and 2-naphthalenethiol, was mixed with an equimolar amount of **1b** (15 μM) and JMJD2E (15 μM) in ammonium acetate (15 mM, pH 7.5) under aerobic conditions. The mixture was then analyzed for binding with

JMJD2E (mass 41264 Da) by nondenaturing ESI-MS. New complexes with peaks at 41587 and 41557 Da were observed (Figure S1, Supporting Information); these peaks correspond to the addition of disulfides **1b**·3-methoxythiophenol (**2a**) and **1b**·thiophenol (**2b**) to JMJD2E, respectively. This result was confirmed by deletion experiments in which specific thiols were removed from the mixture. Because disulfides are not necessarily stable under the FDH coupled assay conditions, the carbon analogues, **3a** and **3b**, respectively, wherein the disulfide bond is replaced with a C−S bond, were then synthesized (Figure 2). Both **3a** and **3b** bind to JMJD2E, as shown by nondenaturing ESI-MS. The FDH coupled assay results indicate that both carbon analogues **3a** (IC$_{50}$ = 204 μM) and **3b** (IC$_{50}$ = 300 μM) are less potent as JMJD2E

inhibitors compared to the support compound **1b** (IC$_{50}$ = 73 μM). This difference could be due to the differences in interactions in solution and in nondenaturing ESI-MS conditions or the inability of the carbon compounds to mimic the S−S bond in disulfides. Nonetheless, the DCMS method revealed that larger side-chains than those of *N*-oxalyl-D-cysteine could likely be accommodated in subpocket of the JMJD2E active site.

It was noted that disulfide **2a** binds slightly more strongly to JMJD2E than **2b**, indicating that the presence of the methoxy group may improve inhibitory activity. This led us to consider using *N*-oxalyl-D-tyrosine **1c** as a lead for further optimization of the aromatic ring. Consequently, a set of *N*-oxalyl-D-tyrosine derivatives (**5a**−**12**, Figure 4) substituted at the tyrosinyl−OH position with a variety of substituents, including benzoate esters (**5a**−**j**), other aliphatic/aromatic esters (**6a**−**k**), sulfonate esters (**7a**−**j**), aliphatic ethers (**9a**−**i**), β-ketoethers (**8a**−**m**, **11a**−**c**, **12**) and benzyl ethers (**10a**−**q**) were analyzed for binding to, and inhibition of, JMJD2E.

The *N*-oxalyl-D-tyrosine derivatives (**5a**−**12**, Figure 4) were initially screened for binding affinity to JMJD2E by the nondenaturing ESI-MS method. The binding affinity of each compound was classified into one of five rank classes. Competition experiments (data not shown) showed that the top 11 compounds all bound more tightly than either *N*-oxalylglycine **1a** or *N*-oxalyl-D-phenylalanine **1d**.

The *N*-oxalyl-D-tyrosinyl derivatives were then tested (at 100 μM) for activity against JMJD2E using the FDH based coupled assay (Figure 6),[9] and the compounds were ranked by inhibitory potency based on the reduction in initial demethylation rate observed. IC$_{50}$s were then determined for nine of the most potent compounds **7f**, **7c**, **7e**, **10k**, **7d**, **8m**, **6d**, **10e**, **10a**, and three of the least potent compounds **7i**, **8b**, and **9h** as a control (Table 1). The most potent compound in the FDH coupled assay was **7f**, with an IC$_{50}$ of 5.4 μM; other potent compounds also had IC$_{50}$s in the low micromolar range (8−40 μM). This represents an improvement of potency with respect to *N*-oxalylglycine **1a** (IC$_{50}$ = 24 μM), *N*-oxalyl-D-phenylalanine **1d** (IC$_{50}$ = 320 μM), and *N*-oxalyl-D-homophenylalanine **1h** (IC$_{50}$ = 39 μM).[9]

The rankings of binding affinity as determined by nondenaturing ESI-MS and inhibitory potency by the FDH coupled assay were compared using Kendall's rank correlation (τ_B = 0.58, p < 0.0001) and Spearman's rank correlation (ρ = 0.72, p < 0.0001). These results indicate a statistically significant positive correlation between the inhibitor rankings by nondenaturing ESI-MS and by FDH coupled assay activity (Figure 5b). Because there are differences in the physical interactions between ligand and enzyme in the gas phase as opposed to solution phase (in gas phase, ionic interactions and hydrogen bonding interactions are believed to be preserved more efficiently than hydrophobic interactions),[19] inhibitors which rely on nonionic interactions for binding to the enzyme in solution may show relatively weaker binding affinity in the mass spectrometric screen. Nonetheless the results reveal that screening for binding by nondenaturing ESI-MS is an efficient and useful method for ranking affinity, which is amenable to medium-throughput analyses and displays a strong correlation to the FDH coupled assay inhibition data.

The most potent inhibitors identified by these screens (**7f**, **7c**, and **7e**, as well as previously described inhibitors **1a** and **1d**) were also screened against PHD2 by nondenaturing ESI-MS binding affinity assays and biochemical activity assays (hydroxylation of CODD peptide substrate by
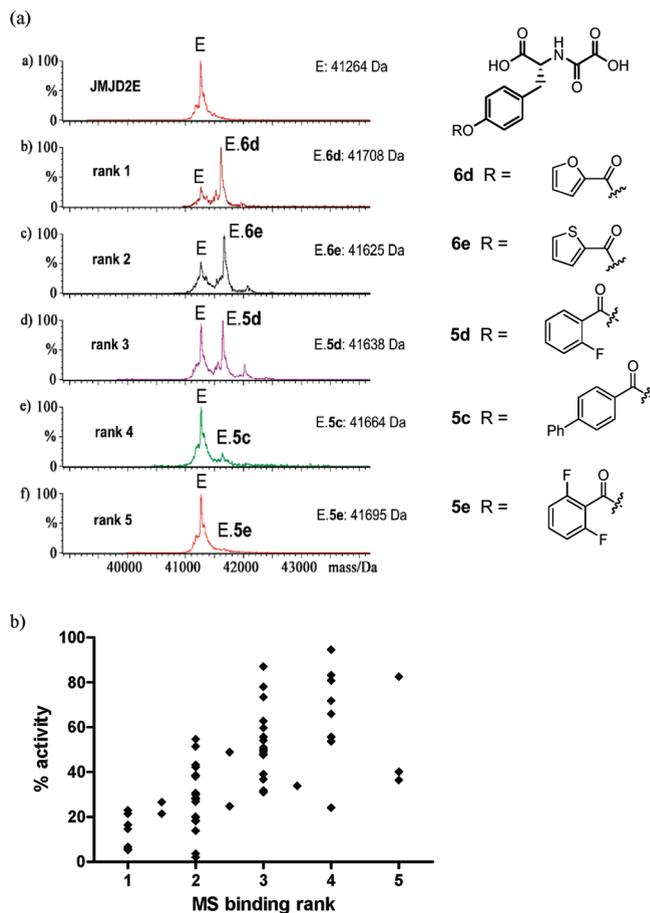

Figure 5. Correlation of nondenaturing ESI-MS analyses and inhibition results for JMJD2E inhibitors. (a) Compounds were grouped in five ranking sets reflecting the strength of binding to the JMJD2E·Fe(II)·Zn(II) complex (**E**). Rank 1: ~1:4 ratio unbound:bound; rank 2: ~1:2 unbound:bound; rank 3: ~1:1 unbound:bound; rank 4: ~4:1 unbound:bound, and rank 5: ~10:1 unbound:bound. The MS spectra show examples of data for representative compounds from each ranking set. Some samples (11 of the 73 compounds tested) were not considered to produce spectra of sufficient quality for classification and were thus excluded from the ranking. (b) Initial rates of all compounds tested as JMJD2E inhibitors (100 μM) binding rank as determined by ESI-MS, demonstrating correlation between the two data sets. Kendall's τ_B = 0.58 (p < 0.0001), Spearman's ρ = 0.72 (p < 0.0001).

PHD2, analyzed by MALDI-TOF MS[27]). No inhibitory activity toward PHD2 was observed in the biochemical assay for the three *N*-oxalyl-D-tyrosine derivatives **7f**, **7c**, and **7e** or for **1d**; *N*-oxalylglycine **1a**, however, was a potent inhibitor of PHD2 as previously reported.[28−31] Some binding was observed between these inhibitors and PHD2 by nondenaturing ESI-MS. However, nondenaturing ESI-MS binding assays in the presence of the known potent inhibitor **1a** showed binding of both **1a** and either **7f**, **7c**, and **7e** simultaneously, suggesting that binding of these *N*-oxalylamino acids was not occurring in the 2OG binding site of the enzyme. Thus, these inhibitors are selective for the JMJD2 HDMs over the human prolyl hydroxylase PHD2. This result is consistent with the lack of a large pocket adjacent to the 2OG side chain binding site in PHD2 as opposed to that observed for JMJD2A.[18,32,33]

Compounds **7f** and **7c** were also screened against FIH using a MALDI-TOF assay as reported.[34] Dose−response curves representing the extent of hydroxylation as a function of inhibitor concentration were used to determine IC$_{50}$s. Both of
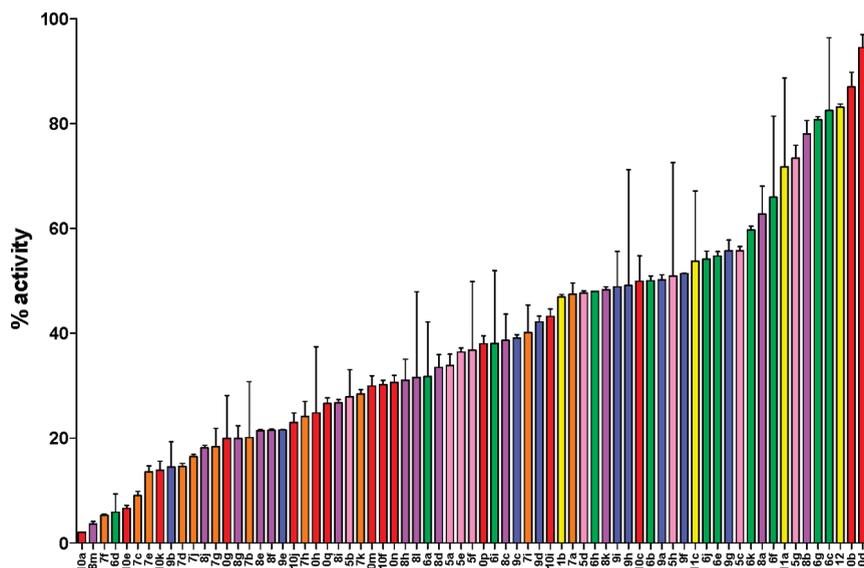
Figure 6. Screening for JMJD2E inhibitors. Compounds were tested as JMJD2E inhibitors (100 μM) using the FDH assay, and the percentage activities relative to the DMSO control are shown. Measurements were made in duplicate and shown as averages with standard errors of the mean.

these compounds, **7f** and **7c** (IC$_{50}$ values for JMJD2E of 5.4 and 8.6 μM, respectively), inhibited FIH with IC$_{50}$ values of 60.2 and 37.2 μM, respectively. Note that direct comparisons of IC$_{50}$ values determined for JMJD2E and FIH should be treated with caution because the assay used for FIH relies on measurement of hydroxylation after a significantly longer incubation period rather than those used in JMJD2E FDH coupled assay. However, the results suggest that, at least for compounds **7f** and **7c**, selectivity of inhibition with regard to FIH was relatively low as might be expected based on the similarity of its 2OG binding subpocket to that of the JMJD2s (Figure S2, Supporting Information).

Crystallization of the most potent *N*-oxalyl-D-tyrosine inhibitors (Table 1) together with JMJD2A was then attempted, and a crystal structure was obtained for compound **10a** in complex with JMJD2A to 2.4 Å resolution (Figure S3 and Table S2, Supporting Information), confirming the predicted binding mode for *N*-oxalyl-D-tyrosinyl derivatives. **10a** was observed to be bound to the active site of both the JMJD2A molecules that are present in the asymmetric unit. The oxalyl carbonyl oxygen and one of the carboxylic acid oxygens of **10a** chelate the active site metal in a manner analogous to 2OG and *N*-oxalylglycine **1a** (avg. 2.2 Å) (Figures 7, 8). The other carboxylic acid of **10a** forms a salt bridge with Lys206 *N*$^{\varepsilon}$ (2.8 Å) and a hydrogen bond with Tyr132 OH (2.4 Å). Apparent hydrophobic interactions between the tyrosinyl side chain of **10a** and JMJD2A include side chains of residues Ile71, Tyr132, Tyr177, Phe185, and Lys241 (methylenes). The tyrosinyl side-chain oxygen of **10a** is positioned to make a weak hydrogen bond (3.7 Å) with the backbone amide nitrogen of Ala186. All residues involved in binding **10a** are conserved between JMJD2A (used for crystallographic analysis) and JMJD2E (presently more amenable to biochemical inhibition assays), and the most potent JMJD2E inhibitors displayed activity against JMJD2A in a MS-based turnover assay (Table 2).

Comparison of the JMJD2A:**10a** crystal structure with the JMJD2A-H3K9me3 substrate complex (PDB ID 2OQ6) revealed little difference in the conformation of the active site residues (Supporting Information Table S5). When the JMJD2A:H3K9me3 substrate complex structure is

Table 1. IC$_{50}$ Values for the Most Potent Compounds Tested (**7f**, **7c**, **7e**, **10k**, **7d**, **8m**, **10e**, **6d**, **10a**), and for Three Less Potent Compounds (**7i**, **8b**, **9h**) (JMJD2E Concentration = 2 μM)

compd	IC$_{50}$ (μM)	ratio of JMJD2E−inhibitor complex to free JMJD2E (by ESI-MS)
7f	5.4	4.3
7c	8.6	poor spectrum
7e	11.7	poor spectrum
10k	14.7	3.1
7d	14.7	5.7
8m	14.8	2.0
10e	16.6	3.6
6d	20.1	3.5
10a	37.1	1.7
7i	82.9	1.0
8b	185.1	0.9
9h	326.5	0.9

superimposed on the JMJD2A:**10a** structure (Figure 9), no overlap is observed between the inhibitor side chain and the substrate K9me3 side chain (Supporting Information Figure S3). However, the benzyl ether moiety of **10a** is observed to partially occupy the same space as Thr11 and Gly12 of the H3K9me3 substrate, indicating that the binding of **10a** (and probably the other potent inhibitors) to JMJD2A likely interferes with binding of the H3K9me3 substrate in addition to competing with 2OG.

To investigate the rationale for the increased potency of the sulfonates **7c**−**f** relative to the other derivatives, inhibitors **7f**, **10k**, **6d**, and **8m** were manually modeled into the active site of the JMJD2A:**10a** structure by superimposing their structures with **10a** and altering the position of each tyrosine substituent to reduce steric clashes and to maximize hydrogen bonding interactions (Figure S4 and Table S3, Supporting Information). All compounds were constrained to form a hydrogen bond between the tyrosinyl oxygen and the backbone amide nitrogen of Ala186, as observed in the JMJD2A:**10a** structure (Figure S4). In all of these compounds, additional hydrogen bonds were predicted to occur compared to those observed in the JMJD2A:**10a** crystal structure. Modeling studies also suggest reasons why **7i**, **8b**, and **9h** are less potent
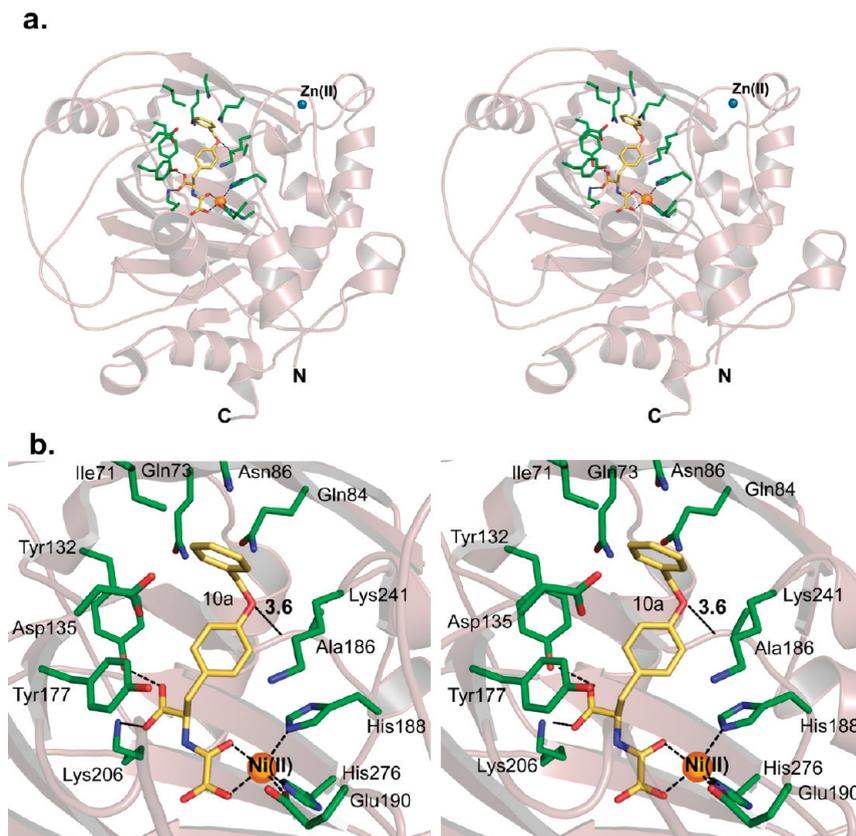
a.

b.

Figure 7. Stereoviews from the JMJD2A:**10a** crystal structure. (a) Stereoview of the crystal structure of JMJD2A (transparent ribbons and green sticks) in complex with compound **10a** (yellow sticks). Ni(II) (orange sphere) replaces Fe(II) in the active site; the structural Zn(II) is shown as a blue sphere. Highlighted residues (green) chelate active site metal and form part of the substrate/cosubstrate binding pocket. (b) Close-up stereoview of substrate/cosubstrate binding site with compound **10a**, showing details of hydrogen bonding interactions between **10a**, Lys206 and Tyr132 side chains, and the backbone amide nitrogen of Ala186.
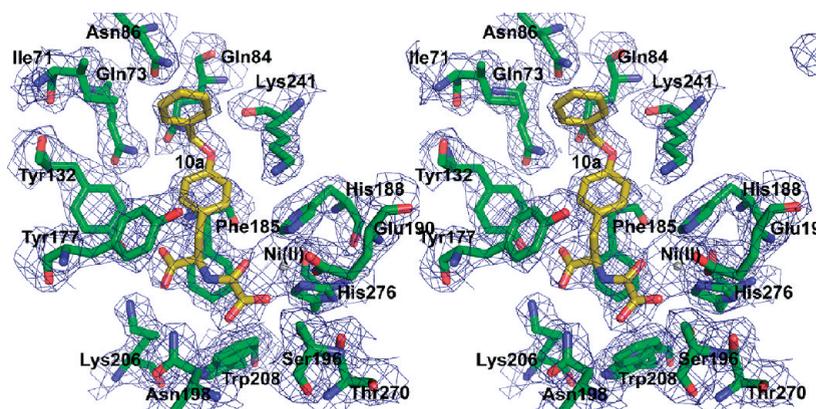

Figure 8. Electron density map (stereoview) showing compound **10a** (yellow sticks) in the active site of JMJD2A (green sticks). The experimental $2F_o - F_c$ electron density, displayed as blue mesh, is shown for the metal (gray sphere) coordinating residues and ligands (contoured to 1σ).

inhibitors: steric interaction in the case of **7i** and **8b**, and conformational flexibility in the case of **9h**.

Taken together, our results indicate that a combined approach involving nondenaturing ESI-MS binding assays to identify hits followed by biochemical assays provides an efficient approach to lead identification of inhibitors for metallo-enzymes. The statistical correlation between the binding strength of compounds to the enzyme under nondenaturing ESI-MS conditions and the ability of compounds to inhibit enzyme activity in biochemical assays validates the nondenaturing ESI-MS method although it is appreciated

that binding strength under noncatalytic conditions does not necessarily reflect inhibitory potency. One advantage of a binding-type assay is that it can be used to identify (potential) inhibitors in the absence of a catalytic turnover assay which requires knowledge of the substrate (substrates are not yet known for many of the 2OG oxygenases).[35]

Our work has also identified inhibitors selective for inhibition of the JMJD2 histone demethylase subfamily members over the HIF hydroxylase PHD2, in that the most potent inhibitors of JMJD2E did not inhibit PHD2 (within the limits of detection), as predicted from structural comparisons

Table 2. Inhibition Data for JMJD2A with Selected Compounds by the MALDI-TOF Assay[a]

compd	JMJD2E IC$_{50}$ by FDH assay (μM)	JMJD2E IC$_{50}$ by MALDI-TOF (μM)	JMJD2A IC$_{50}$ by MALDI-TOF (μM)
7f	5.4	21	12
7c	8.6	61	13
7e	11.7	38	20
10k	14.7	47	14
7d	14.7	43	17
8m	14.8	59	13
10e	16.6	25	10
10a	37.1	76	33
7i	82.9	ND	ND
8b	185.1	ND	ND
9h	326.5	ND	ND

[a] JMJD2A was used at 2 μM, 2OG at 10 μM and ARKme3STGGK peptide at 10 μM. JMJD2E IC$_{50}$s were also determined by MALDI-TOF MS for comparison. ND = not determined.
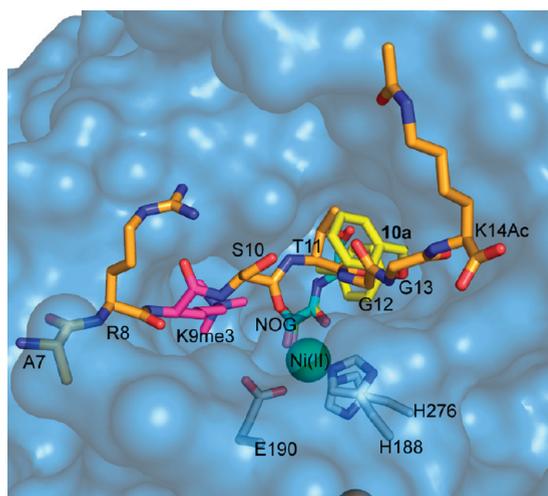

Figure 9. Binding of **10a** to JMJD2A likely interferes with both 2OG and histone substrate binding. Superimposition of H3K9me3 substrate (orange and pink sticks) with JMJD2A·Ni(II)·Zn(II).**10a** structure (PDB ID 2OQ6) is shown. The surface of JMJD2A (blue) illustrates separate K9me3 (pink) and cosubstrate (NOG, cyan, replaces 2OG in this structure) subpockets. Compound **10a** (yellow sticks) occupies a large hydrophobic pocket adjacent to the substrate binding cleft. It may interfere with binding of the Thr11 side chain of the H3K9 substrate.

of the binding pockets. Binding within the identified JMJD2 subpocket may be a way of achieving more potent inhibition with other series of "template" inhibitors that bind to the active site iron. These compounds may be useful as chemical tools to probe the in vivo roles of the JMJD2 demethylases. However, those inhibitors screened against FIH did inhibit HIF asparaginyl hydroxylation, demonstrating that further expansion of this, or related series of compounds that chelate the active site iron, is required to achieve higher selectivity within the JmjC subfamily. In this regard, it is notable that although both FIH and the JMJD2 demethylases contain a relatively large subpocket, there are significant differences in the residues that form these subpockets.

Experimental Section

All reagents and solvents were purchased from Aldrich or Alfa Aesar and used without further purification. Reactions were monitored by TLC, which was performed on precoated aluminum-backed plates (Merck, silica 60 F254). Melting points were determined using a Leica Galen III hot-stage melting point apparatus and microscope. Infrared spectra were recorded from Nujol mulls between sodium chloride discs on a Bruker Tensor 27 FT-IR spectrometer. NMR spectra were acquired using a Bruker DPX500 NMR spectrometer. Chemical shifts (δ) are given in ppm, and the multiplicities are given as singlet (s), doublet (d), triplet (t), quartet (q), multiplet (m), and broad (br). Coupling constants J are given in Hz to the nearest 0.1 Hz. High resolution mass spectra (HRMS) were recorded using Bruker MicroTOF. The purity of all compound synthesized were >95% as determined by analytical reverse-phase HPLC (Ultimate 3000).

The chemical synthesis and purity of **3a** and **3b** are described in the Supporting Information. The 73 N-oxalyl-D-tyrosine derivatives were purchased from ChemOvation (Horsham, UK). The identity and purity of the lead compounds were confirmed by ^{1}H NMR, HRMS, and HPLC (for all compounds), and these data (for compounds **6d**, **7c**, **7d**, **7e**, **7f**, **7i**, **8b**, **8m**, **9h**, **10a**, **10e**, and **10k**) are given in the Supporting Information.

The catalytic domain of human JMJD2E (residues 1−337) was produced as N-terminally His$_6$-tagged protein in *Escherichia coli* and purified by Ni-affinity chromatography as reported.[18]

JMJD2E inhibition was assessed using a FDH coupled assay, as reported.[9] All compounds were initially tested at 100 μM, and the initial rates of demethylation measured by measuring NADH production using an Envision multilabel reader (Perkin-Elmer, Waltham, MA).

For JMJD2A, a MALDI-TOF MS based assay was used becuase JMJD2A was not optimized for analysis in our current FDH assay. JMJD2A 2 μM, Fe(II) 10 μM, and ascorbate 100 μM in 50 mM HEPES pH 7.5 with inhibitor stock DMSO solutions where final inhibitor concentrations varied but final DMSO concentration was always 5% of assay mix were incubated for 15 min at 25 °C, after which time reactions were initiated by addition of 2OG (10 μM) and peptide (10 μM), followed by 30 min incubation at 37 °C. Reactions were quenched with methanol 1:1 (v/v) followed by addition of four volumes of 20 mM triammonium citrate. The diluted assay mixture (1 μL) was then mixed with 1 μL of α-cyano-4-hydroxycinnamic acid (the MAL-DI-TOF-MS matrix) and spotted onto a MALDI-TOF-MS plate.[18] The relative intensities of different methylation states observed in the mass spectra were then used to calculate percentage demethylation. IC$_{50}$s were calculated from the variation in percentage demethylation at different inhibitor concentrations.

FIH and PHD2 assays were carried out as reported.[27,34] The binding of compounds to JMJD2E was evaluated by nondenaturing ESI-MS as described.[9] His-tagged JMJD2E was desalted using a Bio-Spin 6 Column (Bio-Rad, Hemel Hempstead, UK) in 15 mM ammonium acetate pH 7.5. The stock solution was diluted with the same buffer to a final concentration of 100 μM. FeSO$_4$·7H$_2$O was dissolved in 20 mM HCl at a concentration of 100 mM. This was then diluted with Milli-Q water to give final working concentrations of 100 μM. The protein (15 μM) was mixed with 1 equiv of Fe(II) and 1 equiv of inhibitor and incubated for 30 min at 37 °C prior to nondenaturing ESI-MS analysis. For competition experiments, the protein was mixed with equimolar amounts of Fe(II) and two inhibitors each at concentration of 15 μM and incubated for 30 min at 37 °C prior to nondenaturing ESI-MS analysis. Data were acquired on a Q-TOF mass spectrometer (Q-TOF micro, Micromass, Altrincham, UK) interfaced with a Nanomate (Advion Biosciences, Ithaca, NY) with a chip voltage of 1.70 kV and a delivery pressure 0.25 psi (1 psi = 6.81 kPa). The sample cone voltage was typically 80 V, with a source temperature of 40 °C and with an acquisition/ scan time of 10 s/1 s. Calibration and sample acquisition were performed in the positive ion mode in the range of 500−5000 m/z. The pressure at the interface between the atmospheric source and the high vacuum region was fixed at 6.60 mbar. External instrument calibration was achieved by using sodium iodide. Data were processed with MASSLYNX 4.0 (Waters). The limit of detection

by this assay is an IC$_{50}$ of ~1 μM because the JMJD2E enzyme concentration required to achieve sufficient sensitivity in the current assay conditions is 2 μM.

Statistical analyses on correlation between MS and % inhibition rankings were carried out using Kendall's τ_B and Spearman's rank correlation tests, using StatsDirect, http://www.statsdirect.com.

Crystals of JMJD2A:**10a** were grown by vapor diffusion at 4 °C in 200 nL sitting drops, with a 1:1 protein to reservoir solution ratio. The JMJD2A protein solution for crystallization was composed of 11.0 mg/mL protein, 10 mM HEPES pH 7.5, 500 mM NaCl, 5% v/v glycerol, and 0.75 mM **10a**. The reservoir solution included 0.1 M citrate pH 5.5, 18.5% w/v polyethylene glycol 3350, 4 mM NiCl$_2$. The crystals were cryoprotected by transferring to 25% v/v glycerol in well solution and flash frozen by rapidly plunging in liquid nitrogen. Data were collected from a single crystal at 100 K at the Diamond Light Source beamline I03 using 0.97860 Å wavelength beam. The data were processed with MOSFLM and SCALA.[36] Iterative rounds of model building in COOT[37] and refinement using REFMAC[36] resulted in the final model with R = 18.1% and R_{free} = 24.8%. All residues were in acceptable regions of a Ramachandran plot as calculated by MolProbity.[38] Refinement details are shown in Table S2 of the Supporting Information.

Supporting Information Available: Compound quality analyses, inhibition assay methods, mass spectrometric data, and crystallization and structure solution methods. This material is available free of charge via the Internet at http://pubs.acs.org.

References

(1) Klose, R. J.; Zhang, Y. Regulation of histone methylation by demethylimination and demethylation. *Nat. Rev. Mol. Cell Biol.* **2007**, *8* (4), 307–318.

(2) Cloos, P. A.; Christensen, J.; Agger, K.; Helin, K. Erasing the methyl mark: histone demethylases at the center of cellular differentiation and disease. *Genes Dev.* **2008**, *22* (9), 1115–1140.

(3) Tsukada, Y.; Fang, J.; Erdjument-Bromage, H.; Warren, M. E.; Borchers, C. H.; Tempst, P.; Zhang, Y. Histone demethylation by a family of JmjC domain-containing proteins. *Nature* **2006**, *439* (7078), 811–816.

(4) Cloos, P. A.; Christensen, J.; Agger, K.; Maiolica, A.; Rappsilber, J.; Antal, T.; Hansen, K. H.; Helin, K. The putative oncogene GASC1 demethylates tri- and dimethylated lysine 9 on histone H3. *Nature* **2006**, *442* (7100), 307–311.

(5) Fodor, B. D.; Kubicek, S.; Yonezawa, M.; O'Sullivan, R. J.; Sengupta, R.; Perez-Burgos, L.; Opravil, S.; Mechtler, K.; Schotta, G.; Jenuwein, T. JMJD2B antagonizes H3K9 trimethylation at pericentric heterochromatin in mammalian cells. *Genes Dev.* **2006**, *20* (12), 1557–1562.

(6) Klose, R. J.; Kallin, E. M.; Zhang, Y. JmjC-domain-containing proteins and histone demethylation. *Nat. Rev. Genet.* **2006**, *7* (9), 715–727.

(7) Whetstine, J. R.; Nottke, A.; Lan, F.; Huarte, M.; Smolikov, S.; Chen, Z.; Spooner, E.; Li, E.; Zhang, G.; Colaiacovo, M.; Shi, Y. Reversal of histone lysine trimethylation by the JMJD2 family of histone demethylases. *Cell* **2006**, *125* (3), 467–481.

(8) Katoh, M.; Katoh, M. Identification and characterization of JMJD2 family genes in silico. *Int. J. Oncol.* **2004**, *24* (6), 1623–1628.

(9) Rose, N. R.; Ng, S. S.; Mecinović, J.; Liénard, B. M. R.; Bello, S. H.; Sun, Z.; McDonough, M. A.; Oppermann, U.; Schofield, C. J. Inhibitor Scaffolds for 2-Oxoglutarate-Dependent Histone Lysine Demethylases. *J. Med. Chem.* **2008**, *51* (22), 7053–7056.

(10) Edwards, A. M.; Bountra, C.; Kerr, D. J.; Willson, T. M. Open access chemical and clinical probes to support drug discovery. *Nat. Chem. Biol.* **2009**, *5* (7), 436–440.

(11) Spannhoff, A.; Hauser, A. T.; Heinke, R.; Sippl, W.; Jung, M. The emerging therapeutic potential of histone methyltransferase and demethylase inhibitors. *ChemMedChem* **2009**, *4* (10), 1568–1582.

(12) Schofield, C. J.; Ratcliffe, P. J. Oxygen sensing by HIF hydroxylases. *Nat. Rev. Mol. Cell Biol.* **2004**, *5* (5), 343–354.

(13) Schofield, C. J.; Ratcliffe, P. J. Signalling hypoxia by HIF hydroxylases. *Biochem. Biophys. Res. Commun.* **2005**, *338* (1), 617–626.

(14) Kaelin, W. G., Jr.; Ratcliffe, P. J. Oxygen sensing by metazoans: the central role of the HIF hydroxylase pathway. *Mol. Cell* **2008**, *30* (4), 393–402.

(15) McDonough, M. A.; McNeill, L. A.; Tilliet, M.; Papamicael, C. A.; Chen, Q. Y.; Banerji, B.; Hewitson, K. S.; Schofield, C. J. Selective inhibition of factor inhibiting hypoxia-inducible factor. *J. Am. Chem. Soc.* **2005**, *127* (21), 7680–7681.

(16) Clissold, P. M.; Ponting, C. P. JmjC: cupin metalloenzyme-like domains in jumonji, hairless and phospholipase A2beta. *Trends Biochem. Sci.* **2001**, *26* (1), 7–9.

(17) Hewitson, K. S.; McNeill, L. A.; Riordan, M. V.; Tian, Y. M.; Bullock, A. N.; Welford, R. W.; Elkins, J. M.; Oldham, N. J.; Bhattacharya, S.; Gleadle, J. M.; Ratcliffe, P. J.; Pugh, C. W.; Schofield, C. J. Hypoxia-inducible factor (HIF) asparagine hydroxylase is identical to factor inhibiting HIF (FIH) and is related to the cupin structural family. *J. Biol. Chem.* **2002**, *277* (29), 26351–26355.

(18) Ng, S. S.; Kavanagh, K. L.; McDonough, M. A.; Butler, D.; Pilka, E. S.; Lienard, B. M. R.; Bray, J. E.; Savitsky, P.; Gileadi, O.; von Delft, F.; Rose, N. R.; Offer, J.; Scheinost, J. C.; Borowski, T.; Sundstrom, M.; Schofield, C. J.; Oppermann, U. Crystal structures of histone demethylase JMJD2A reveal basis for substrate specificity. *Nature* **2007**, *448* (7149), 87–91.

(19) Loo, J. A. Studying noncovalent protein complexes by electrospray ionization mass spectrometry. *Mass. Spectrom. Rev.* **1997**, *16* (1), 1–23.

(20) Lienard, B. M. R.; Selevsek, N.; Oldham, N. J.; Schofield, C. J. Combined Mass Spectrometry and Dynamic Chemistry Approach to Identify Metalloenzyme Inhibitors13. *ChemMedChem* **2007**, *2* (2), 175–179.

(21) Lienard, B. M.; Huting, R.; Lassaux, P.; Galleni, M.; Frere, J. M.; Schofield, C. J. Dynamic combinatorial mass spectrometry leads to metallo-beta-lactamase inhibitors. *J. Med. Chem.* **2008**, *51* (3), 684–688.

(22) Mecinovic, J.; Chowdhury, R.; Lienard, B. M.; Flashman, E.; Buck, M. R.; Oldham, N. J.; Schofield, C. J. ESI-MS studies on prolyl hydroxylase domain 2 reveal a new metal binding site. *ChemMedChem* **2008**, *3* (4), 569–572.

(23) Mecinovic, J.; Loenarz, C.; Chowdhury, R.; Schofield, C. J. 2-Oxoglutarate analogue inhibitors of prolyl hydroxylase domain 2. *Bioorg. Med. Chem. Lett.* **2009**, *19* (21), 6192–6195.

(24) Poulsen, S. A. Direct screening of a dynamic combinatorial library using mass spectrometry. *J. Am. Soc. Mass Spectrom.* **2006**, *17* (8), 1074–1080.

(25) Maresca, A.; Temperini, C.; Vu, H.; Pham, N. B.; Poulsen, S.-A.; Scozzafava, A.; Quinn, R. J.; Supuran, C. T. Non-Zinc Mediated Inhibition of Carbonic Anhydrases: Coumarins Are a New Class of Suicide Inhibitors. *J. Am. Chem. Soc.* **2009**, *131* (8), 3057–3062.

(26) Lienard, B. M.; Garau, G.; Horsfall, L.; Karsisiotis, A. I.; Damblon, C.; Lassaux, P.; Papamicael, C.; Roberts, G. C.; Galleni, M.; Dideberg, O.; Frere, J. M.; Schofield, C. J. Structural basis for the broad-spectrum inhibition of metallo-beta-lactamases by thiols. *Org. Biomol. Chem.* **2008**, *6* (13), 2282–2294.

(27) Flashman, E.; Bagg, E. A.; Chowdhury, R.; Mecinovic, J.; Loenarz, C.; McDonough, M. A.; Hewitson, K. S.; Schofield, C. J. Kinetic rationale for selectivity toward N- and C-terminal oxygen-dependent degradation domain substrates mediated by a loop region of hypoxia-inducible factor prolyl hydroxylases. *J. Biol. Chem.* **2008**, *283* (7), 3808–3815.

(28) Epstein, A. C.; Gleadle, J. M.; McNeill, L. A.; Hewitson, K. S.; O'Rourke, J.; Mole, D. R.; Mukherji, M.; Metzen, E.; Wilson, M. I.; Dhanda, A.; Tian, Y. M.; Masson, N.; Hamilton, D. L.; Jaakkola, P.; Barstead, R.; Hodgkin, J.; Maxwell, P. H.; Pugh, C. W.; Schofield, C. J.; Ratcliffe, P. J. *C. elegans* EGL-9 and mammalian homologs define a family of dioxygenases that regulate HIF by prolyl hydroxylation. *Cell* **2001**, *107* (1), 43–54.

(29) Hirsila, M.; Koivunen, P.; Gunzler, V.; Kivirikko, K. I.; Mylly-harju, J. Characterization of the human prolyl 4-hydroxylases that modify the hypoxia-inducible factor. *J. Biol. Chem.* **2003**, *278* (33), 30772–30780.

(30) Mole, D. R.; Schlemminger, I.; McNeill, L. A.; Hewitson, K. S.; Pugh, C. W.; Ratcliffe, P. J.; Schofield, C. J. 2-Oxoglutarate analogue inhibitors of HIF prolyl hydroxylase. *Bioorg. Med. Chem. Lett.* **2003**, *13* (16), 2677–2680.

(31) Jaakkola, P.; Mole, D. R.; Tian, Y. M.; Wilson, M. I.; Gielbert, J.; Gaskell, S. J.; Kriegsheim, A.; Hebestreit, H. F.; Mukherji, M.; Schofield, C. J.; Maxwell, P. H.; Pugh, C. W.; Ratcliffe, P. J. Targeting of HIF-alpha to the von Hippel−Lindau ubiquitylation complex by O₂-regulated prolyl hydroxylation. *Science* **2001**, *292* (5516), 468–472.

(32) Chowdhury, R.; McDonough, M. A.; Mecinovic, J.; Loenarz, C.; Flashman, E.; Hewitson, K. S.; Domene, C.; Schofield, C. J. Structural basis for binding of hypoxia-inducible factor to the oxygen-sensing prolyl hydroxylases. *Structure* **2009**, *17* (7), 981–989.

(33) McDonough, M. A.; Li, V.; Flashman, E.; Chowdhury, R.; Mohr, C.; Lienard, B. M.; Zondlo, J.; Oldham, N. J.; Clifton, I. J.; Lewis, J.; McNeill, L. A.; Kurzeja, R. J.; Hewitson, K. S.; Yang, E.; Jordan, S.; Syed, R. S.; Schofield, C. J. Cellular oxygen sensing: Crystal structure of hypoxia-inducible factor prolyl hydroxylase (PHD2). *Proc. Natl. Acad. Sci. U.S.A* **2006**, *103* (26), 9814–9819.

(34) Hewitson, K. S.; Holmes, S. L.; Ehrismann, D.; Hardy, A. P.; Chowdhury, R.; Schofield, C. J.; McDonough, M. A. Evidence that two enzyme-derived histidine ligands are sufficient for iron binding and catalysis by factor inhibiting HIF (FIH). *J. Biol. Chem.* **2008**, *283* (38), 25971–25978.

(35) Loenarz, C.; Schofield, C. J. Expanding chemical biology of 2-oxoglutarate oxygenases. *Nat. Chem. Biol.* **2008**, *4* (3), 152–156.

(36) Collaborative Computational Project, Number 4. The CCP4 suite: programs for protein crystallography. *Acta Crystallogr., Sect. D: Biol. Crystallogr.* **1994**, *50*, 760−763.

(37) Emsley, P.; Cowtan, K. *Acta Crystallogr., Sect. D: Biol. Crystallogr.* **2004**, *60*, 2126–2132.

(38) Davis, I. W.; Leaver-Fay, A.; Chen, V. B.; Block, J. N.; Kapral, G. J.; Wang, X.; Murray, L. W.; Arendall, W. B., III; Snoeyink, J.; Richardson, J. S.; Richardson, D. C. MolProbity: all-atom contacts and structure validation for proteins and nucleic acids. *Nucleic Acids Res.* **2007**, *35* (Web Server Issue), W375–W383.